Original Article

Therapeutic potential of epiphyseal growth plate cells for bone regeneration in an osteoporosis model

Journal of Tissue Engineering
Volume 13: 1–13

DOI: 10.1177/20417314221116754
journals.sagepub.com/home/tej
SAGE

Inho Baek[1], Alvin Bacero Bello[1], Jieun Jeon[1], Yoshie Arai[1], Byung-Hyun Cha[2], Byoung Ju Kim[3] and Soo-Hong Lee[1]

Abstract

Bone growth occurs in the epiphyseal growth plate (EGP) and epiphyseal growth plate cells (EGPCs) exist in EGP. EGPCs, including skeletal stem cells (SSCs), are cells that induce bone growth and development through endochondral ossification. Recently, the superiority of bone regeneration through endochondral ossification has been reported. Our study compared EGPCs with bone marrow-derived mesenchymal stem cells (BM-MSCs) and suggested the therapeutic potential of new bone regeneration. In this study, we analyzed the characteristics between EGPCs and BM-MSCs based on morphological characteristics and molecular profiles. EGPCs expressed chondrogenic and osteogenic markers higher than BM-MSCs. Additionally, in co-culture with BM-MSCs, EGPCs induced an increase in chondrogenic, osteogenic, and hypertrophic markers of BM-MSCs. Finally, EGPCs induced higher bone regeneration than BM-MSCs in the osteoporosis model. Overall, we suggest the possibility of EGPCs as cell therapy for effective bone regeneration.

Keywords

Epiphyseal plate, growth plate cells, endochondral ossification, osteoporosis, bone regeneration

Date received: 2 March 2022; accepted: 14 July 2022

Introduction

Bone formation in a developing embryo begins with the mesenchyme and occurs through one of two processes—either endochondral or intramembranous ossification (osteogenesis). These two types of ossification ensue *via* different molecular processes, but both ultimately lead to bone formation.[1] Intramembranous ossification involves direct bone formation, *via* the differentiation of mesenchymal stem cells (MSCs) into osteoblasts. Most of the cranial bones are primarily formed via intramembranous ossification.[2] In contrast, endochondral ossification involves the hypertrophy of a cartilaginous template into bone tissue. These processes generally occur in two major regions, the diaphysis and epiphysis. First, a primary ossification center is formed in the diaphysis as blood vessels and osteoblasts infiltrate and replace the calcified cartilaginous template.[3] This process is then followed by a secondary ossification in the epiphysis. Upon completion of the bone formation, un-calcified hyaline cartilage is constricted and remains only in a cell reservoir called the epiphyseal growth plate (EGP) and in the articular regions.[4,5] In the process of development, most bones, except the cranial bones, are formed *via* endochondral ossification.[6]

In long bones, the epiphyseal cartilaginous growth plate is largely divided into four main zones—the resting,

[1]Department of Medical Biotechnology, Dongguk University, Goyang, Gyeonggi, Republic of Korea
[2]Division of Biomedical Convergence, College of Biomedical Science, Kangwon National University, Chuncheon, Republic of Korea
[3]ATEMs, Seoul, Republic of Korea

Corresponding authors:
Soo-Hong Lee, Department of Medical Biotechnology, Dongguk University, 32 Dongguk-ro, Ilsandong-gu, Goyang, Gyeonggi 10326, Republic of Korea.
Email: soohong@dongguk.edu

Byoung Ju Kim, ATEMs, 9th floors, 7, Jeongui-ro 8-gil, Songpa-gu, Seoul 05836, Republic of Korea.
Email: kbz9861@hanmail.net

proliferative, pre-hypertrophic, and hypertrophic zones. To regenerate the bone, non-dividing chondrocytes in the resting zone undergo a sequence of events, which include rapid proliferation and differentiation, for *de novo* bone formation to replace the old tissue. The resting zone is a key region of the EGP because it contains several populations of stem cells that can regenerate old tissues. Among the cell types that reside in this region, skeletal stem cells (SSCs) are determined to differentiate into osteocyte and then contribute to bone structures. SSCs have been reported to have a higher capacity to differentiate into bone or cartilage than any other stem cells.[7] Interestingly, epiphyseal growth plate cells (EGPCs) contain cells expressing CD200, a representative surface marker of SSCs. These CD200-positive EGPCs are known as stem cells and have high proliferation, differentiation, and regeneration ability.[8] And thus EGPCs may be a reliable replacement for adult stem cells in therapeutic applications for bone regeneration. Also, it has been shown that the endochondral process generates bone regeneration with higher density and flexible bones than intramembranous process.[9–11] Since SSCs are directly involved in endochondral ossification,[12] we hypothesize that SSCs-rich EGPCs are superior to adult stem cells for bone regeneration. Thus, in this study, we aimed to investigate whether EGPCs are able to show higher bone regeneration capability as compared to BM-MSCs.

Materials and methods

Isolation and culture of EGPCs and BM-MSCs from rats

EGPCs and BM-MSCs were isolated from 8 weeks old Sprague Dawley (SD) male rat. All the animal procedures were performed in accordance with a protocol approved by the institutional Animal Care and Use Committee (IACUC) of Dongguk University (IACUC 2019-047-2). The male, 7 weeks old Sprague Dawley (SD) Rats were purchased from Orient Bio, Inc (Seongnam, Korea). Animals were raised at 55%–65% humidity and a controlled temperature of 20°C–24°C with a light/dark cycle of 12 h/12 h. Rats had free access to food and water ad libitum. All rats were sacrificed in a CO_2 gas chamber.

We obtained rat EGPCs through surgical methods from the EGPs of the tibiae plateau and femoral condyle. All the cells of the entire epiphyseal plate (all four layers) were isolated. To obtain the cells from the EGP, the tissue was incubated with 0.3% type II collagenase in Low Glucose-Dulbecco's Modified Eagle's Medium (LG-DMEM; Hyclone) at 37°C for 2 h. Isolated EGPCs were filtered through a 0.4 μm strainer, and the collagenase solution was removed by washing the cells with Dulbecco's phosphate-buffered saline (DPBS). Subsequently, the cells were seeded in a 100 mm dish. Cells were isolated from the femur EGP tissue of eight rats. The EGPCs were cultured in the LG-DMEM media supplemented with 10% Fetal Bovine Serum (FBS; Gibco) and 1% Antibiotic-Antimycotic (100X) (AA; Gibco) medium, with medium changes every 2 days.

For rat BM-MSCs, the bone marrows of the tibiae plateau and femoral condyle were harvested and collected into Dulbecco's Modified Eagle's Medium (DMEM, Hyclone). The cells were then filtered through a 40 μm filter and centrifuged at 1300 rpm for 3 min. After rinsing the cells with DPBS three times, they were maintained in LG-DMEM supplemented with 10% FBS and 1% AA. BM-MSCs were incubated at 37°C in humidified air with 5% CO_2. After 12 h of culture, the cells were washed with DPBS and cultured with the maintenance medium (DMEM supplemented with 10% FBS and 1% AA), which was changed every 2–3 days. The cells were passaged at 80% confluence. Isolated EGPCs and BM-MSCs cultured up to passage four were used in all the experiments.

Cell proliferation

The proliferative capacities of BM-MSCs and EGPCs were measured via the Cell Counting Kit-8 assay (CCK-8, Dojindo, Japan). Cells were seeded at a concentration of 4000 cells per well into a 24-well plate and cultured with DMEM. To quantitate cell proliferation, the cells in each well were treated with a 1:10 mix of medium and CCK-8. After 1 h of incubation, the absorbance of the media was measured using Cytation 3 (BioTek).

Flow cytometry

Cell-membrane expression of the MSC markers CD73, CD44, and CD90 and the SSC marker CD200 on BM-MSCs and EGPCs were analyzed *via* flow cytometry. Cells in culture were washed with DPBS twice and detached using 0.25% trypsin. They were then collected by centrifugation. The cell pellets were re-suspended in DPBS with 2% FBS (FACS buffer), incubated with specific primary antibodies for 30 min at 4°C, and then washed with the FACS buffer three times. Antibodies against CD73 (NBP2-25235; 5′-Nucleotidase/CD73 Antibody, NOVUS BIOLOGICALS), CD44 (MCA643GA; MOUSE ANTI RAT CD44, Bio-Rad, UK), CD90 (sc-53456; Thy-1/CD90 antibody (aTHy-1A1), Santa Cruz Biotechnology), and CD200 (MA1-70035; CD200 Monoclonal Antibody (OX-2), ThermoFisher Scientific) were used as the primary antibodies (1:100 diluted in the FACS buffer). The cells were then washed with the FACS buffer twice and incubated with the secondary antibodies (1:100 diluted in the FACS buffer; Mouse IgG ($H + L$) Cross-Adsorbed Secondary Antibody (A-11001) in Immunohistochemistry (IHC), ThermoFisher Scientific) for 30 min at 4°C in the FACS buffer. The cells were finally washed with the FACS buffer three times, and their

Table 1. Primer pairs used for qRT-PCR.

Gene	Ref seq no.	Forward	Reverse
18S	NM_046237.1	GTA ACC CGT TGA ACC CCA TT	CCA TCC AAT CGG TAG TAG CG
Sox9	NM_080403.1	TTT GCA GTG TTT TCC GCC AC	TGC AGA AGC TTG CGT TGT TC
Acan	XM_039101035.1	GAC ACC CCT ACC CTT GCT TC	TCA CAT TGC TCC TGG TCT GC
Col2a1	NM_012929.1	GCC AGG ATG CCC GAA AAT TAG	GTC ACC TCT GGG TCC TTG TTC
Runx2	NM_001278484.2	CCA CAG AGC TAT TAA AGT GAC AGT G	AAC AAA CTA GGT TTA GAG TCA TCA AGC
Ocn	NM_013414.1	GCT CAA CCC CAA TTG TGA CG	GGG CAA CAC ATG CCC TAA AC
Col1a1	NM_053304.1	CAT GTT CAG CTT TGT GGA CCT	GCA GCT GAC TTC AGG GAT GT
Opn	NM_012881.2	CGG TGA AAG TGG CTG AGT TT	GGC TAC AGC ATC TGA GTG TTT G
Pparγ	NM_001145366.1	CCC AAT GGT TGC TGA TTA CA	GGA CGC AGG CTC TAC TTT GA
Apn	NM_144744.3	AAA TGT GGA GCC AGG CCT CT	ACA CTT GGA GCC AGA CTT GG
Glut4	NM_012751.1	CGA CGG ACA CCT TCT CTC TT	AGG GCT AAA GTG CTG CGA G
Mmp2	NM_031054.2	AGG GCA GTG GGA TAC AGG T	GCC GTA AGG GAG ACA CCA G
Mmp8	NM_022221.1	CCC TGA CCT TCA CTG AGA CC	CAT CAA ATG GAG AAT TGT CAC C
Mmp13	NM_133530.1	GAA ACC TGG ACA AGC AGC TC	GTC CAG ACC GAG GGA GTG
Bmp7	NM_001191856.2	GTC TGC TCA GAA GAG GTC GG	CAC GTC CCT CCC ACC TTC A
Ihh	NM_053384.1	CTC AGA CCG CGA CCG AAA TA	AAT ACA CCC AGT CGA AGC CG
Col10a1	XM_001053056.8	CGA TCA TGG AGC TCA CGG AA	AGG AGT AGA GGC CGT TCG AT

fluorescence was detected by using BD Accuri C6 (BD Science). Background fluorescence was subtracted after analyzing unstained cells and cells stained only with the corresponding isotype controls.

Quantitative reverse transcription–polymerase chain reaction (qRT-PCR)

To quantitate the multi-differentiation potentials of rat BM-MSCs and EGPCs, total RNA was extracted from the cells, and the mRNA levels of various differentiation markers were measured *via* qRT-PCR. The list of the primers used is shown in Table 1. Total RNA was isolated *via* the conventional Trizol method (Gibco Invitrogen, CA). Cells were incubated with Trizol reagent at room temperature (20°C–30°C) for 5 min and were collected in Eppendorf tubes. Then 200 µl chloroform was added to the cell mixture and incubated on ice for 15 min. The mixture was centrifuged at 13,000 rpm for 15 min. The aqueous supernatant was gently collected and mixed with the same volume of isopropanol and incubated in ice for 10 min. The RNA sample was centrifuged at 13,000 rpm for 15 min and the supernatant was discarded. The RNA pellet was washed with 75% EtOH and air-dried. The transparent RNA pellet was re-suspended in nuclease-free water. RNA concentration was measured using Cytation 3, and 1 µg total RNA was converted to cDNA by using the PrimeScript RT Reagent kit (TAKARA, Japan). qPCR analyses were performed using the Power Syber Green PCR Master Mix (ThermoFisher Scientific) with the cDNA samples (1:10 diluted) and 10 pmol gene-specific primers. The ΔΔCT value was measured using a Step-One perfect qPCR machine (ThermoFisher Scientific). The samples were subjected to the following PCR conditions: denaturation for 15 s at 95 °C, followed by 40 cycles of 30 s denaturation at 95°C, annealing at 60°C for 1 min, and extension at 72°C for 30 s.

Western blotting

Chondrogenic, osteogenic, and adipogenic protein expression in rat BM-MSCs and EGPCs were measured by western blotting. Total protein was extracted by incubating the cells in Radioimmunoprecipitation assay (RIPA) buffer. The protein concentrations were quantified using the BicinChoninate Acid (BCA) protein assay, and 25 ng/µl protein samples were separated by denaturing 10% Polyacrylamide gel electrophoresis (PAGE) and transferred to nitrocellulose membranes. The membranes were blocked with 5% non-fat skim milk (BD Difco) in Tris-Buffered Saline (TBS) with 1% Triton X-100 (TBST) for 1 h and subsequently incubated with primary antibodies (1:500–1000 dilution for SOX9, ACAN, COL2A1, RUNX2, COL1A1, OCN, PPARγ, APN, and GLUT4) in TBST with 5% bovine serum albumin (BSA) overnight at 4°C. The list of the antibodies used is shown in Table 2. The membranes were washed and then incubated for 2 h at room temperature with the secondary antibody (goat anti-mouse or anti-rabbit conjugated to horse radish peroxidase) diluted 1:5000 in TBST with 5% non-fat skim milk. Immunoreactive bands were detected using E-select (Amersham™, UK), and images were visualized using the Bio-Rad Image Lab software.

Co-culture of BM-MSCs with EGPCs

The two chambers of a trans-well were separated by a semi-permeable membrane with a pore size of 0.4 µm (BD

Table 2. List of primary antibodies used in Western blotting analysis.

Antigen	Type	Dilution	Manufacturer	Catalog number
Sox9	Rbp	1:1000	Novus biologicals	NBP1-85551
Acan	Rbp	1:1000	Abcam	ab36861
Col2a1	RbP	1:700	invitrogen	PA1-26206
RUNX2	RbM	1:1000	Cell signaling	mAb8486S
OCN	Rbp	1:1000	millipore	AB10911
Col1a1	Rbp	1:700	Abcam	ab34710
PPARγ	Rbp	1:1000	Abcam	ab19481
APN	MM	1:1000	R&D systems	MAB3100-SP
GLUT4	Rbp	1:1000	Novus biologicals	NBP1-49533

MM: mouse monoclonal; Rbp: rabbit polyclonal; RbM, rabbit monoclonal.

Biosciences). BM-MSCs and EGPCs were cultured in the upper chamber of the trans-well inserts while the bottom chamber contained only BM-MSCs. Cells were cultured and analyzed up to 7 days. Upon completion of the co-culture, the differentiation of the BM-MSCs in the bottom chamber was evaluated. Gene-expression levels were assessed *via* qRT-PCR.

Bone puncture in an animal model of osteoporosis

A total of 31 female 8 week-old Sprague Dawley Rats were purchased from Orient Bio, Inc. All the animal experiments were approved by the Institutional Animal Care and Use Committee of Dongguk University (IACUC-2019-047-2). Animals were raised at 55%–65% humidity and a controlled temperature of 20°C–24°C with a light/dark cycle of 12 h/12 h. Rats had free access to food and water ad libitum. After 1 week of stabilization, 31 mice were subjected to ovariectomy (OVX) procedure. All animals were anesthetized with a mixture of tiletamine hydrochloride/zolazepam hydrochloride (Zoletil, 50 mg/kg, Virbac Laboratories, France) and xylazine (Rompun, 10 mg/kg, Bayer, Korea) in saline. The ovaries of 25 female rats were removed through a single ventral transverse incision.[13–15] Injection was performed twice at 2 and 4 weeks after OVX, respectively. A hole with a diameter of 0.2 mm was made on the long bones by using a twist drill (Jeung Do Bio & Plant Co., Seoul, Korea). All the rats were randomly divided into the following five experimental groups: group 1, sham ($n=6$); group 2, OVX ($n=7$); group 3, OVX + 20 µl hyaluronic acid (HA) hydrogel (Hyruan Plus®, LG life sciences, Iksan, Korea) ($n=6$); group 4, OVX + 20 µl HA hydrogel + BM-MSCs (1×10^6 cells) ($n=6$); and group 5, OVX + 20 µl HA hydrogel + EGPCs (1×10^6 cells) ($n=6$). BM-MSCs or EGPCs with HA hydrogel were injected into the long-bone cavity by using a 1 ml insulin syringe with a staked 29-gage needle (Shina Corp., Seoul, Korea). For multiple injections, groups 3–5 were injected two times at 2 and 4 weeks, respectively. And the animals were sacrificed at 6 weeks after OVX. All rats were sacrificed in a CO_2 gas chamber.

Micro computed tomography (CT)

Microstructural change in the femur long bone was evaluated using a Skyscan 1172 Micro-CT (Skyscan, Kontich, Belgium) 6 weeks after the treatment. The X-ray source was set to a voxel size of 6.96 µm at 59 keV and 167 µA. The exposure time was 440 ms with a frame average of three. X-ray beam filtration made of 0.5 mm aluminum was used.[16] Data were recorded at every 0.4° of the rotation step until 180°. Image slices were reconstructed by using the NRecon software (Skyscan) based on the Feldkamp algorithm, and by applying a correction for the beam. The bone mass in the long bones was chosen as the region of interest (ROI). For these ROIs, the three-dimensional bone-volume fraction (BV/TV), trabecular thickness (Tb.Th), bone trabecular number (Tb.N, 1/mm), bone trabecular separation (Tb.Sp, mm), and structure model index (SMI) were calculated.[17]

Histological analysis

After Micro-CT scanning, the operated femoral long bones were fixed in 10% Neutral buffered formalin for 72 h. They were then decalcified in 10% nitric acid solution for 24 h at 4°C and embedded in paraffin. The embedded samples were cut into 5 µm sections by using a microtome (Leica Microsystems RM2245, Wetzlar, Germany). The sections were de-paraffinized using xylene and ethanol and washed with phosphate-buffered saline (PBS). The sections were stained with Hematoxylin and Eosin, Safranin-O, Fast Green, or Masson's trichrome stain to evaluate the chondrogenic and bone formation. The stained sections were washed with PBS three times and visualized using an inverted microscope (Olympus, Japan).

Statistical analysis

The data are representative of three independent experiments with each experiment done in triplicate. Error bars denote the means ± standard deviation (SD) and the differences with p values <0.05 were considered statistically significant (ns: not significant, $*p<0.05$, $**p<0.01$, $***p<0.001$). One-way analysis of variance (ANOVA) followed by Tukey's post hoc test was used to compare the mean values among groups. Individual data points and p-values for significance are indicated in the graph.

Results

Characterization of EGPCs and BM-MSCs

EGPCs were obtained from the femur and tibia (Figure 1). The EGP was revealed by removing the long-bone head, called the CAP. Only the cells in the upper part of the EGP were collected.[7,18,19]

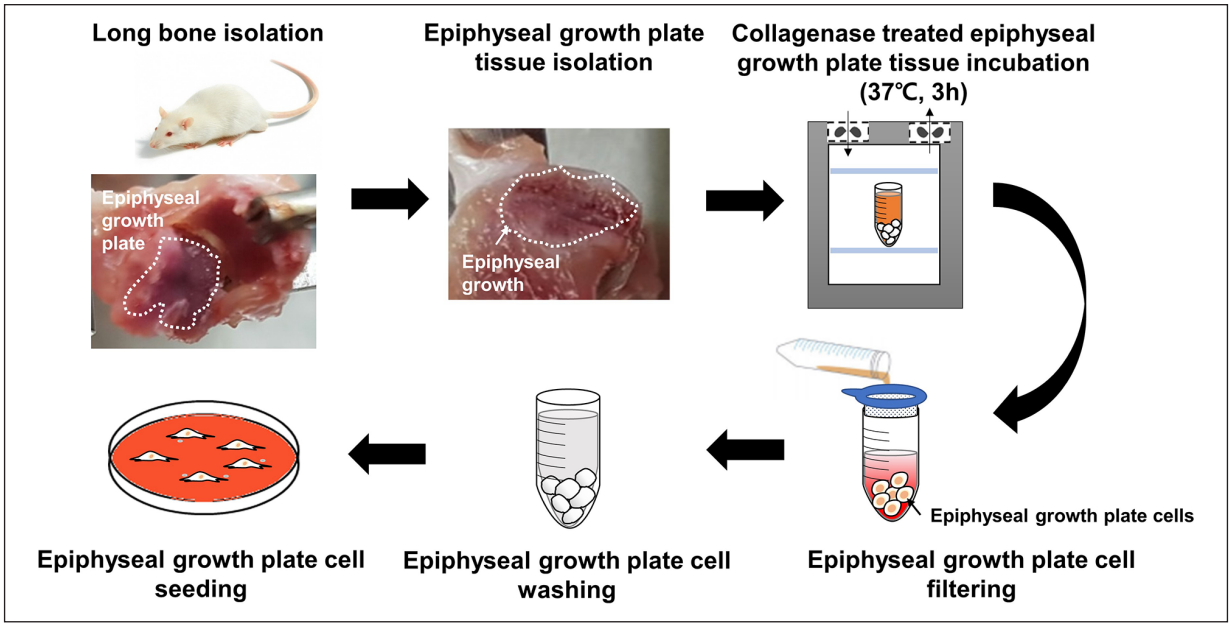

Figure 1. Graphical abstract of the isolation of EGPCs from the tibia and femur of rats.

We characterized EGPCs compared to BM-MSCs of rats. The morphology of EGPCs and BM-MSCs is shown in Figure 2. BM-MSCs were more elongated than EGPCs, which appeared more compact and rounder than BM-MSCs. The shape of BM-MSCs was defined by long horizontal structures as a spindle-like shape, whereas EGPCs tended to have short and blunt shapes as a cobblestone-like shape without any horizontal structures (Figure 2(a)). Cell proliferation was measured daily for 7 days *via* a CCK-8 kit. Although the morphologies of the two cell populations were different, the proliferation rates were similar (Figure 2(b)). When the cell cycle was analyzed *via* PI staining followed by flow cytometry, it was confirmed that the fractions of cells at the S phase, mitotic stage indicating cell division, were similar between EGPCs and BM-MSCs (3.4% and 3.5%, respectively) (Figure 2(c)).

Immunophenotypic characterization of cell surface was analyzed to confirm the expression of MSC markers, such as CD73, CD44, and CD90.[20] Also, the SSC marker CD200 was also analyzed (Figure 2(d)).[21,22] The MSC markers CD73 and CD90 were significantly lower in EGPCs (CD73: 72.6% and CD44: 96.9%) compared with BM-MSCs (CD73: 95.7% and CD44: 97.0%). Interestingly, MSC marker CD90 was detected at very low level in EGPCs (CD90: 5.2%). However, CD90 expression of BM-MSCs was detected at 88.1%. On the other hand, the SSC marker CD200 is expressed at a higher level in EGPCs (41%) than in BM-MSCs (11%). These results suggest that EGPCs and BM-MSCs have different characteristics regarding morphological shape and cellular surface molecule expression, especially CD200.

Skeletogenic (chondrogenic and osteogenic) potentials of EGPCs and BM-MSCs

To determine the characteristics of EGPCs, qRT-PCR was performed to measure the expression levels of various chondrogenic, osteogenic, and adipogenic gene markers (Figure 3(a)–(c)). We observed that EGPCs had significantly higher mRNA expression levels of the chondrogenic markers SPY-Box transcription factor 9 (*SOX9*), aggrecan (*ACAN*), and type 2 collagen (*COL2A1*), and the osteogenic markers runt-related transcription factor 2 (*RUNX2*), osteocalcin (*OCN*), and type 1 collagen (*COL1A1*) (Figure 3(a) and (b)). However, as for adipogenesis-specific markers, the basal expression levels of peroxisome proliferator-activated receptor gamma (*PPARγ*), and glucose transporter type 4 (*GLUT4*) were lower in EGPCs than BM-MSCs and adiponectin (*APN*) was not significant (Figure 3(c)). These results were in line with their protein levels. EGPCs showed higher protein levels of ACAN, COL2A1, RUNX2, OCN, and COL1A1 proteins than BM-MSCs (Figure 3(d) and (e)).

This indicates that the growth plate is comprised of cells that are more committed to osteo-chondral rather than to adipogenic lineage. Interestingly, the EGPCs have a higher expression of the osteo-chondral markers compared with BM-MSCs which represents a capacity of skeletogenic differentiation.

Promotion of differentiation and hypertrophy through the paracrine effect of EGPCs

To evaluate the paracrine effect of EGPCs, co-culture was performed with BM-MSCs using a trans-well, and gene

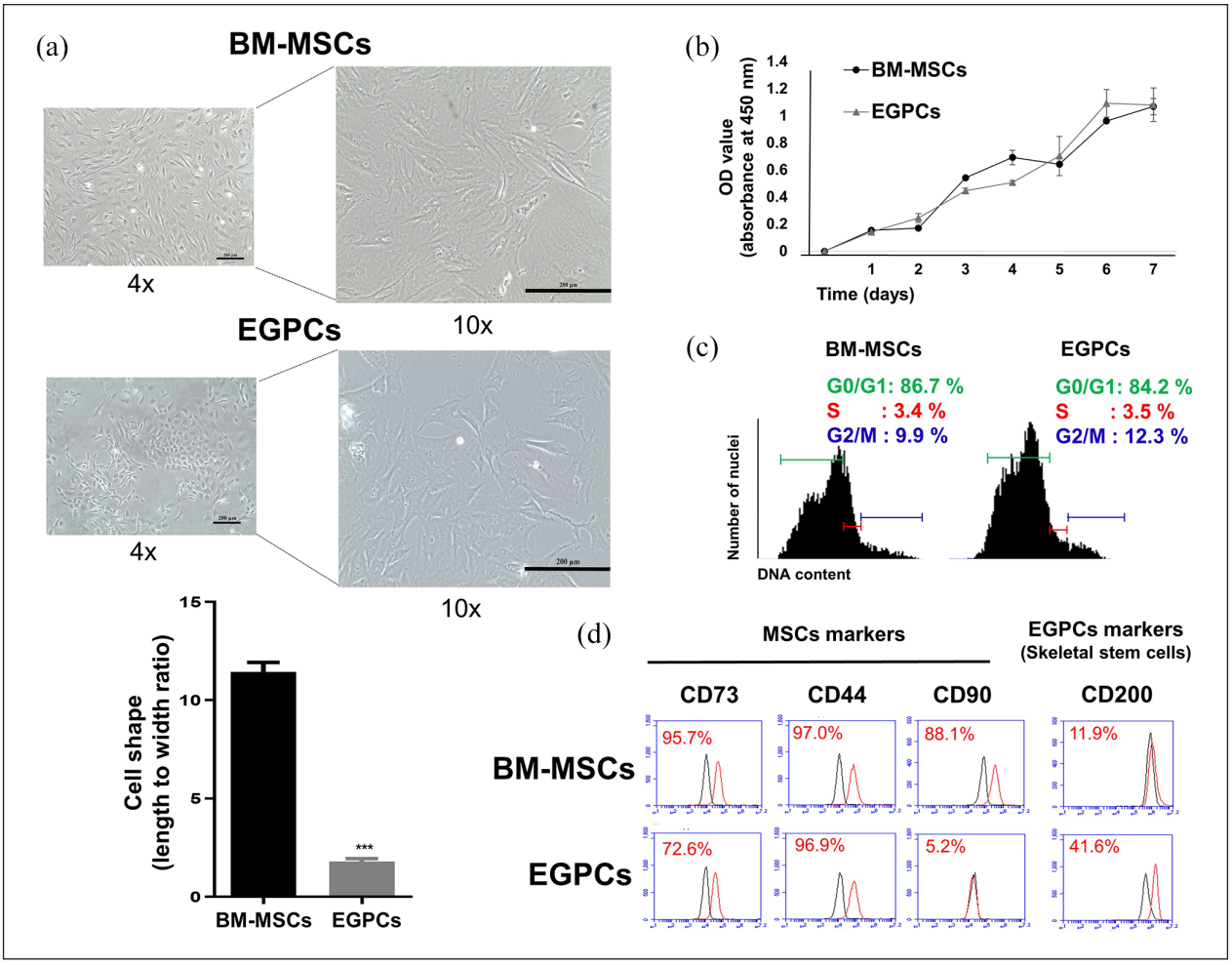

Figure 2. Cellular characterization of EGPCs and BM-MSCs: (a) observation of cell morphology and measurement of cell shape (length to width ratio), (b) the proliferation rates of EGPCs and BM-MSCs were measured from day 1 to day 7 by the CCK-8, (c) cell-cycle analysis of BM-MSCs and EGPCs by using propidium-iodide staining. Quantitation of the cells at each-cycle phase, and (d) Flow-cytometric analyses for the surface markers on BM-MSCs and EGPCs. Representative flow-cytometry profiles are depicted for CD73, CD44, CD90, and CD200. Black and red plots represent the negative control and experimental samples, respectively.

expression was compared at 7 days (Figure 4(a)). Gene expression analyses demonstrated that the BM-MSCs co-cultured with EGPCs induced the higher expression of the chondrogenic markers *SOX9* (6.01 ± 0.130-fold), *ACAN* (6.71 ± 0.113-fold), and *COL2A1* (5.19 ± 0.887-fold) compared to BM-MSCs co-cultured with BM-MSCs (Figure 4(b)). Interestingly, the expression of all chondrogenic markers in the EGPCs co-culture group was significantly high.

We also demonstrated whether EGPCs increase the expression of osteogenic markers in BM-MSCs through the paracrine effect, based on the high expression of osteogenic markers in EGPCs as shown in Figure 3. To investigate this, we evaluated the expression of osteogenic markers such as *RUNX2, OCN*, and *COL1A1* (Figure 4(c)). The EGPCs co-culture group showed a remarkable increase in the expression of *RUNX2* (5.26 ± 0.071-fold) and *OCN* (6.16 ± 0.780-fold) compared to that in the BM-MSCs co-culture group. Due to the characteristics of skeletogenic stem cells, EGPCs not only induced differentiation into chondrogenic cells but also induced osteogenic cells. However, in EGPCs co-culture group, *COL1A1* (0.98 ± 0.004-fold) showed no significant increase. Since this data confirmed the induction of differentiation by EGPCs co-culture group in the basal medium, presumably, strong differentiation could not be induced in a short period of time. We suggest that a sufficient differentiation period is required, as *COL1A1* is a late differentiation marker of osteogenesis.

EGPCs via the paracrine effect have been demonstrated to have skeletogenic related functions but have not identified characteristics related to adipogenic induction (Figure 4(d)). The EGPCs co-culture group showed a low expression of *PPARγ* (0.69 ± 0.004-fold) and a slight increase of *APN* (1.09 ± 0.027-fold) and *GLUT4* (1.64 ± 0.190-fold), but showed no significant difference from the BM-MSCs co-culture group.

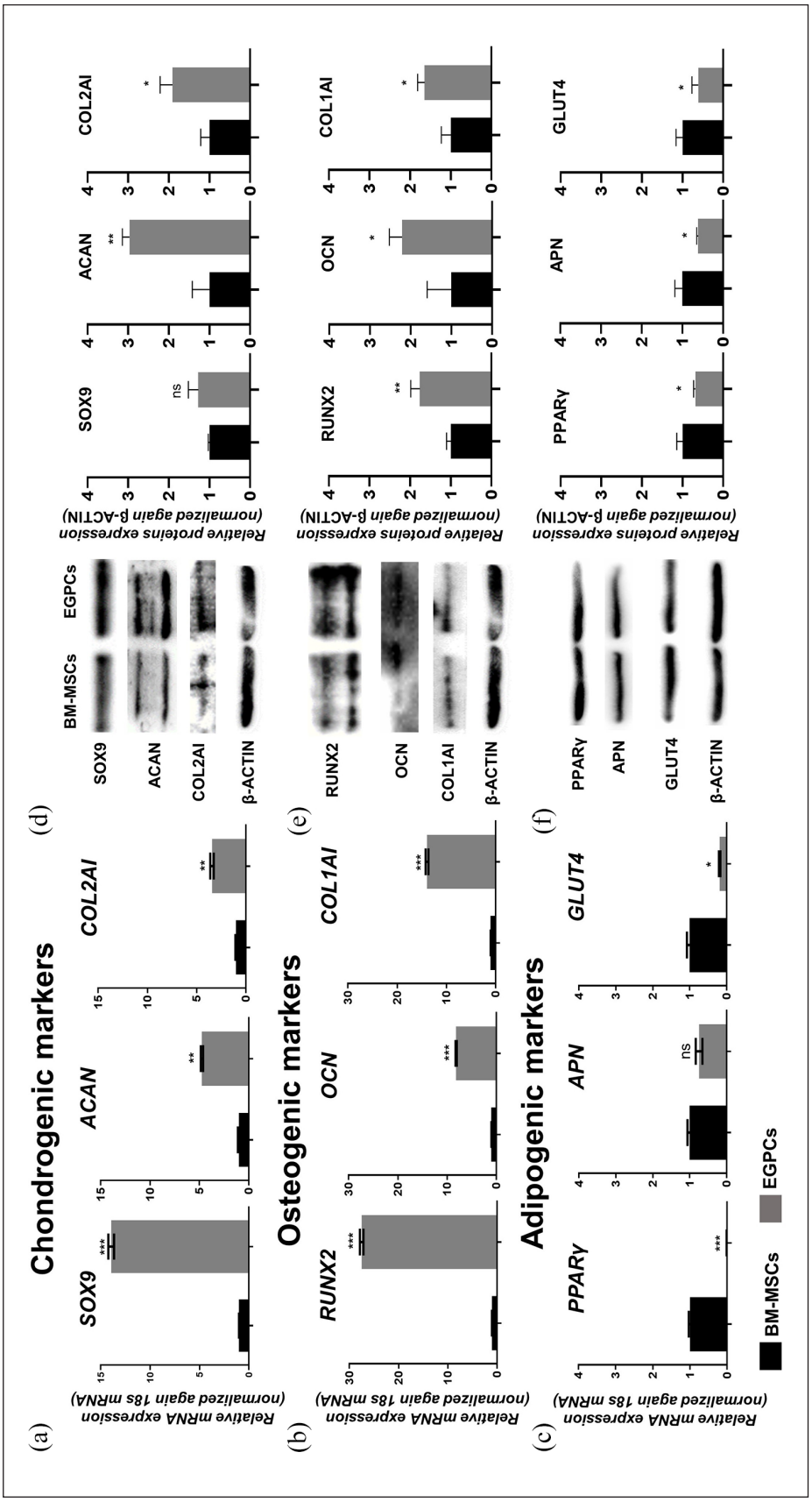

Figure 3. Molecular characterization of EGPCs and BM-MSCs. (a–f) Expression levels of chondrogenic (SOX9, ACAN, and COL2A1), osteogenic (RUNX2, OCN, and COL1A1), and adipogenic (PPARγ, APN, and GLUT4) factors, as assessed via quantitative reverse transcription–polymerase chain reaction (qRT-PCR) and western blotting. qRT-PCR data were normalized against the level of 18S RNA, whereas the western-blot data were normalized against the level of β-ACTIN. The data are representative of two independent experiments performed in triplicate. mean ± SEM; ns: not significant, $^{*}p < 0.05$, $^{**}p < 0.01$, $^{***}p < 0.001$. Individual data points and *p*-values for significance are indicated on the graph.

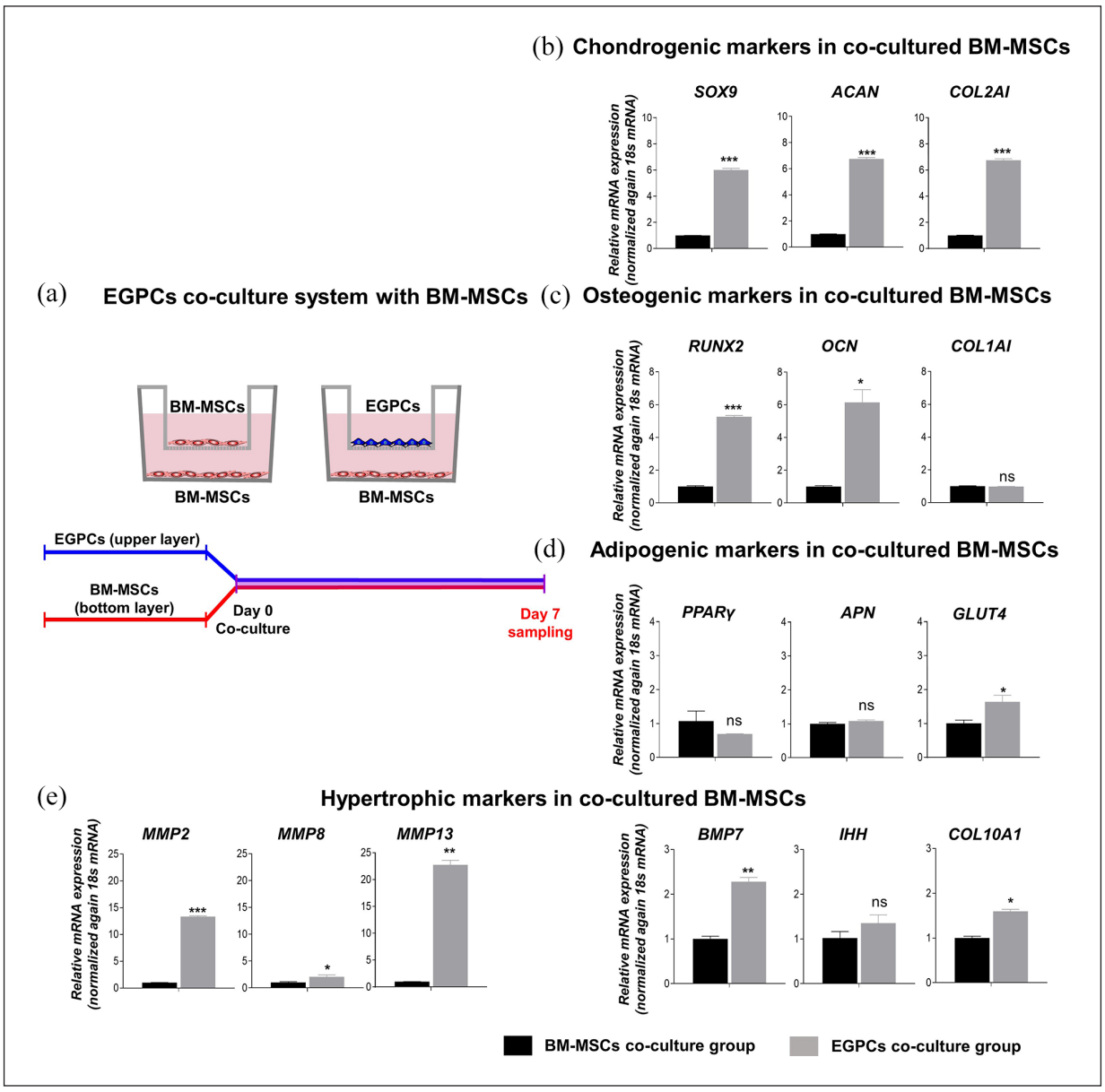

Figure 4. In vitro multi-differentiation potential of bone-marrow–derived mesenchymal stem cells (BM-MSCs) by influence of EGPCs. The establishment of a co-culture trans-well chamber system consisting of BM-MSCs and EGPCs: (a) conceptual diagram of the co-culture of BM-MSCs and EGPCs. The EGPCs and BM-MSCs were seeded in the upper chamber. BM-MSCs were seeded in the bottom chamber (trans-well pore size = 0.4 μm). The differentiation properties of the BM-MSCs in the bottom chamber were analyzed on days 7. (b–e) On days 7 of the co-culture, the mRNA levels of chondrogenic (*SOX9, ACAN*, and *COL2A1*), osteogenic (*RUNX2, OCN*, and *COL1A1*), adipogenic (*PPARγ, APN*, and *GULT4*) markers, and hypertrophic (*MMP2, 8, 13, BMP7, IHH*, and *COL10A1*) markers were measured using qPCR. mean ± SEM; ns: not significant, $*p < 0.05$, $**p < 0.01$, $***p < 0.001$.

Taken together, co-culture study suggests that EGPCs *via* paracrine effect can induce chondrogenic or osteogenic differentiation of surrounding BM-MSCs rather than adipogenic differentiation.

EGPCs co-culture stimulates hypertrophic change of BM-MSCs

In the later stages of bone development through endochondral ossification, hypertrophic change occurs. This is an essential process as it contributes to the growth of long bones and prepares the matrix for vascularization and deposition of new matrix components. We investigated hypertrophy-related markers to demonstrate the association of hypertrophy in endochondral ossification (Figure 4(e)). The EGPCs co-culture showed an increase in the expression of matrix metalloproteinase (MMP) family of proteins such as MMP2 (13.35 ± 0.142-fold), MMP8 (2.10 ± 0.326-fold), and MMP13 (22.76 ± 0.832-fold) compared to that in the BM-MSCs co-culture group.

Additionally, the expression of markers known to be associated with hypertrophy, such as bone morphogenetic protein 7 (*BMP7*) (2.28 ± 0.091-fold) and *COL10A1* (1.60 ± 0.045-fold) was also significantly higher. Our results indicated an increase in hypertrophic markers related to endochondral ossification through the co-culture of EGPCs.

Overall, based on gene expression analysis, EGPCs effectively induced the osteogenic and chondrogenic differentiation of cells, and promotes hypertrophy of BM-MSCs. These results revealed that EGPCs could be utilized to induce the efficient differentiation of BM-MSCs into functional osteo-chondral progenitor cells.

Effects of EGPCs in bone formation in a rat model of osteoporosis

To determine the bone regeneration ability of EGPCs, EGPCs were injected into the long bone of OVX surgery-induced osteoporosis rat model (Figure 5(a)). This osteoporosis model was performed using a routinely used method. The experimental groups were as follows: positive control (Sham), negative control (osteoporosis group, OP), comparison, BM-MSC–treated, and EGPC-treated groups. The results demonstrated that, compared with BM-MSCs and EGPCs groups, osteoporosis-induced rats had a substantially lower trabecular bone volume and number, thinner trabecular thickness, and wider non-bony region (Figure 5(b)).

Based on the micro-CT images, de novo bone formation 6 weeks after the OVX surgery was quantitatively evaluated using many parameters, such as percent bone volume (BV/TV, %), trabecular thickness (Tb.Th), trabecular number (Tb.N), the number of trabecule in a unit length), trabecular separation (Tb.Sp, trabecular spacing), and SMI (Figure 5(c)). The bone parameters were significantly different among the osteoporosis, BM-MSC-treated, and EGPC-treated groups. The percent volume of new trabecular bone formation was significantly higher in the EGPC-treated group than in the BM-MSC–treated group ($15.1\% \pm 3.1\%$ vs $6.7\% \pm 2.2\%$) 6 weeks after the implantation. In addition, trabecular thickness (108.2 ± 8.5 vs $64.5 \pm 12.6\,\mu m$), trabecular number (0.283 ± 0.027 vs 0.201 ± 0.066), and SMI (6.16 ± 0.45 vs 4.55 ± 1.10) were significantly greater in the EGPC-treated group than in the BM-MSC–treated group. Trabecular separation, meaning the non-bony area of the ROI, showed the most similar results to Sham.

Histological analysis of the bone formation occurring via endochondral ossification

The EGPCs group showed superior regenerative effects to the BM-MSCs group based on the results from Hematoxylin & Eosin, Safranin-O, and Masson & Trichrome staining (Figure 5(d)). We demonstrated that the sponge-bone regeneration was confirmed via Masson's trichrome staining. When comparing the bone-regeneration potentials, both the BM-MSCs and EGPCs groups showed significant bone regeneration compared with the osteoporosis groups. However, we found higher bone regeneration in the EGPCs group than in the BM-MSCs group. In the EGPCs group, sponge-bone regeneration showed the most similar results to sham. Also, when analyzing the bone regeneration effect through quantitative analysis of IHC (OCN), the EGPCs group showed the most similar regeneration ability to sham (Figure 5(e)). These results concluded that EGPCs could sufficiently play a biological function *in vivo* and thereby could be used for bone regeneration in osteoporosis.

Discussion

The aim of this study was to compare EGPCs and BM-MSCs, which are known to support bone regeneration, and to suggest the potential of new cell therapy for osteoporosis in EGPCs. EGPCs contain SSCs, specialized stem cells that are committed to differentiate into the skeletogenic (chondrogenic and osteogenic) lineage. SSCs are known to have the potential to regenerate superb bone structures.[18,23,24] Here, we found that the bone regeneration potential of EGPCs containing SSCs was superior to BM-MSCs and determined their capacity as cell therapeutics for osteoporosis. EGPCs have self-renewal ability and multi-differentiation potency specialized for bone/cartilage like BM-MSCs.[24] EGPCs *via* endochondral ossification will be an effective cell therapy for bone diseases such as osteoporosis.

First, as shown in Figure 2, EGPCs had a different shape from BM-MSCs, but their proliferative ability was similar. EGPCs had a short and blunt shape as a cobblestone-like shape than BM-MSCs (Figure 2(a)). In general, the morphology of cell phenotypes supports their function.[25] the BM-MSCs showed typical fibroblast-like morphology as was shown in many previous studies.[26] Our data also showed the fibroblast-like morphology. This result means that our BM-MSCs have the characteristics of traditional MSCs. The blunt-shaped morphology of EGPCs was similar to chondrocytes than fibroblast cells. This study didn't analyze the correlation between morphology and function. However, we suggest that the morphology of EGPCs is similar to bone-related cells. While EGPCs showed similar proliferation capabilities to BM-MSCs (Figure 2(b) and (c)). Flow-cytometry analysis showed that EGPCs had fewer populations of cells with the MSC markers CD73, CD44, and CD90 than BM-MSCs. However, the expression of CD200 as a SSCs marker in EGPCs was shown around 40% that is much higher than that in BM-MSCs (Figure 2(d)). Surface markers are important indicators of cell types and states, and our observations imply that EGPCs are cell s containing SSCs and

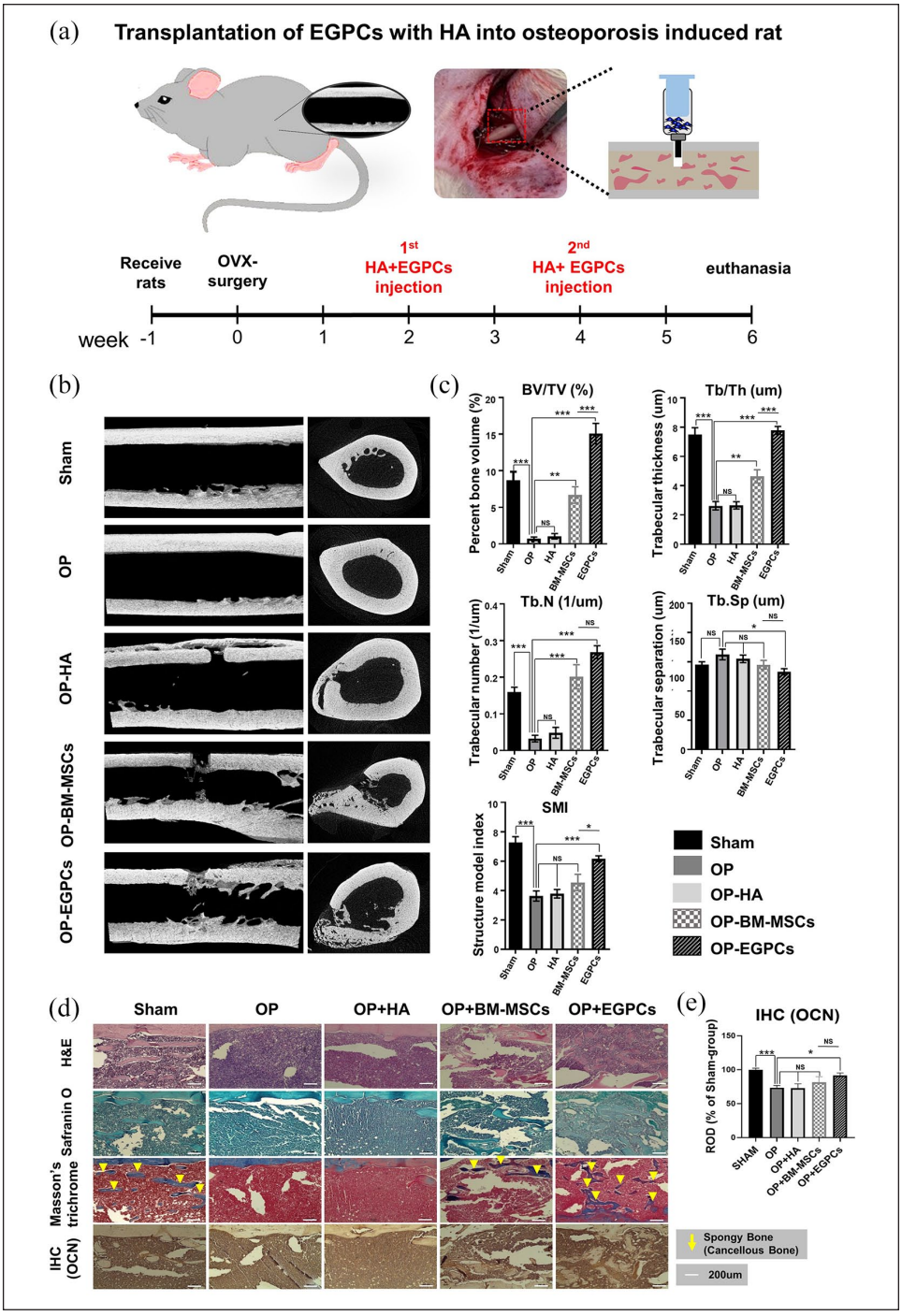

Figure 5. *In vivo* bone regeneration potential of EGPCs in an osteoporosis model: (a) time schedule of *in vivo* experiment for bone formation in the osteoporosis model upon injection of EGPCs and BM-MSCs. Rats received OVX-surgery at 9 weeks of age. They received HA + EGPCs injection on the long bone at 2 and 4 weeks after OVX, respectively. After the end of the experiments, femur was removed and analyzed for micro-CT and bone histo-staining, (b) images of micro computed tomography, demonstrating the three-dimensional (3D) reconstructed image 2 weeks after the last cell injection, (c) bone histomorphometry of the 3D bone formation was analyzed in an ROI for all the groups. The plots of the parameters are structure model index (SMI), percent bone volume (BV/TV, %), trabecular thickness (Tb.Th, μm), trabecular number (Tb.N, 1/μm), and trabecular separation (Tb.Sp, μm); $n = 6$ animals per group, mean ± SEM; ns: not significant, $^{*}p < 0.05$, $^{**}p < 0.01$, $^{***}p < 0.001$, (d) histological evaluation of a rat femur 6 weeks after induced osteoporosis. Hematoxylin in and Eosin staining (upper panel); Safranin O staining (middle panel); Masson's Trichrome staining (bottom panel). In Masson's Trichrome staining, the blue and red colors indicate recently formed and calcified bones, respectively, and (e) quantitative analysis of IHC for OCN. A histogram of OCN staining intensity expressed as relative optical density (ROD) of brown reaction products.

have a similar lineage to BM-MSCs, but with higher biological functions. Indeed, the levels of chondrogenic (*SOX9, ACAN*, and *COL1A1*) and osteogenic (*RUNX2* and *OCN*) markers in EGPCs were significantly higher than that BM-MSCs (Figure 3(a) and (b)). Contrary to this, the levels of adipogenic (*PPARγ* and *GLUT4*) markers were identified to be similar or lower (Figure 3(c)). Our results indicate that EGPCs are skeletogenic cells specialized in bone and cartilage differentiation. This outcome suggests that EGPCs are a lineage of SSCs and have the potential to generate high-quality bone and cartilage tissues through endochondral ossification.[27]

Another important factor for bone regeneration is the surrounding environment. Cell therapy for bone regeneration plays a role in which the injected cells influence the surrounding cells.[19] BM-MSCs inhibit the immune system and promote cell proliferation to enhance bone regeneration.[28–31] In addition, numerous studies have been conducted to prove the hypothesis that enhanced regeneration and differentiation are achieved through the action of paracrine elements in stem cells.[32–34] Strikingly, in our co-culture system, EGPCs affected surrounding cells like BM-MSCs (Figure 4). EGPCs upregulate the levels of chondrogenic, osteogenic, and hypertrophic in BM-MSCs through the paracrine effect. In particular, the significant increase in the expression of chondrogenic (*SOX9, ACAN*, and *COL1A1*) and osteogenic (*RUNX2* and *OCN*) markers demonstrated the potential of EGPCs as effective cell therapeutics (Figure 4(b) and (c)). Along with the expression of chondrogenic and osteogenic markers, hypertrophic markers demonstrated that EGPCs increased the expression of markers in endochondral ossification, such as *MMP2, MMP3, MMP13, BMP7*, and *COL10A1* (Figure 4(e)). This result demonstrates EGPCs are not only able to differentiate into osteocyte during endochondral ossification process, also induce osteogenic differentiation of BM-MSCs presumably due to paracrine factors. It has been reported that principal markers such as *RUNX2, COL10, MMP13, BMP*, and Indian hedgehog (*IHH)* in the hypertrophic region is highly expressed through the endochondral ossification process.[35–39] We have discussed hypertrophic of endochondral ossification in a previous paper. First, the MMP family including the *MMP2, 3*, and *13* degrades the extracellular matrix (ECM) of the cartilage and thus induces bone development. Second, *BMP* is the major pathway regulating cartilage and bone development. Ablation of the type I BMP receptor (BMPR1A) gene in chondrocytes damages cartilage and bone balance, indicating that the BMP act at multiple levels during the bone formation of MSCs. Finally, *IHH* induces chondrocyte hypertrophy and leads to upregulation of *RUNX2*-mediated hypertrophy-related factors, including *COL10* and *MMP13*.[40] Consequently, we believe that these results suggest that the upregulation of hypertrophy markers can induce hypertrophy of chondrocyte to form bones in endochondral ossification. In addition, in the BM-MSCs co-cultured with EGPCs group on days 14, it was shown that gene expression of osteogenic, chondrogenic, and hypertrophic markers was higher than that in the BM-MSCs co-cultured BM-MSCs group (Supplemental Figure S1). In co-culture study confirming paracrine effect, most of studies have been only focusing on early stage, rather than long culture period. Several papers reported that indeed the paracrine effect drastically increases at the early stage, and the effect decreases as time proceeds.[41,42] Although there was no difference between days 7 and 14 in each group, the results were clear that co-culture of EGPCs significantly increases osteogenic markers in day 7 (Figure 4) and day 14 (Supplemental Figure S1).

We also quantified and compared cytokines secreted by EGPCs and BM-MSCs (Supplemental Figure S2). In EGPCs, Stroma-derived growth factor 1 (SDF-1), regulated on activation, normal T cell expressed (RANTES), MMP-9, 13, BMP-2, 7, 9, and interleukin-4, 10 (IL-4, 10), which are cytokines involved in bone induction, were detected higher than BM-MSCs. In addition, the amount of cytokines related to chondrogenic differentiation such as transforming growth factor-β 1, 2, 3 (TGF-β 1, 2, 3), TIMP metallopeptidase inhibitor-1,2 (TIMP-1, 2), matrilin-3, and activin A was significantly higher in EGPCs than in BM-MSCs. Taken together, it was concluded that EGPCs are able to secret a higher amount of cytokines associated with bone and cartilage formation compared to BM-MSCs.

The most important factor in this study is whether EGPCs have effective bone regeneration in the osteoporosis model. We evaluated the bone regeneration capacity of EGPCs in an osteoporosis model (Figure 5(a)). This experiment showed higher BV/TV, Tb.Th, Tb.N, and SMI ratios in EGPC-derived bones than in BM-MSC–derived bones (Figure 5(b) and (c)). Consistent with the micro-CT findings, Masson's trichrome staining of the histological sections showed that a larger area of newly formed spongy bone was achieved with EGPCs than with BM-MSCs (Figure 5(d) and (e)). Considering all these findings, we concluded that EGPCs contributed to the high-quality bone regeneration. Hence, we found that EGPCs, to which the SSC sub-population is the most committed, can enhance osteoporosis-induced bone regeneration. However, it has not been confirmed that EGPCs undergo chondrogenesis during bone regeneration. Therefore, additional studies are needed to verify endochondral ossification by EGPCs.

Conclusion

In summary, BM-MSCs are traditionally used cell therapy for bone regeneration. However, it was less effective in systemic diseases such as osteoporosis. Therefore, stem cells specialized for bone/cartilage regeneration such as SSCs were studied. EGPCs are cells that reside in the resting zone of EGP and contain SSCs. EGPCs express higher

chondrogenic and osteogenic markers than BM-MSCs and have paracrine effects on surrounding cells. Also, EGPCs showed an effect on bone regeneration. By demonstrating higher bone regeneration capacity than BM-MSCs, this study suggests the possibility of EGPCs as cell therapy for effective bone regeneration.

Acknowledgements

We would like to give our sincere appreciation to the reviewers for their helpful comments on this article.

Author Contributions

Soo-Hong Lee conceived and supervised the study. Byoung Ju Kim and Inho Baek designed the study. Inho Baek performed the cell culture and analysis. Byoung Ju Kim and Inho Baek performed the animal experiments. Inho Baek, Alvin Bacero Bello, Yoshie Arai, Byung-Hyun Cha and Jieun Jeon wrote and revised the manuscript. All authors have read and approved the submitted manuscript.

Declaration of conflicting interests

The author(s) declared no potential conflicts of interest with respect to the research, authorship, and/or publication of this article.

Funding

The author(s) disclosed receipt of the following financial support for the research, authorship, and/or publication of this article: This work was supported by the National Research Foundation of Korea (NRF) grant funded by the Korea government (MSIT) (NRF-2019M3A9H1032376, NRF-2019R1C1C1008479 and 2022R1A2C3004850) and the Korea Health Technology R&D Project through the Korea Health Industry Development Institute (KHIDI), funded by the Ministry of Health & Welfare, Republic of Korea(grant number : 21C0703L1)

ORCID iD

Soo-Hong Lee https://orcid.org/0000-0001-6369-8301

Supplemental Material

Supplemental material for this article is available online.

References

1. Ortega N, Behonick DJ and Werb Z. Matrix remodeling during endochondral ossification. *Trends Cell Biol* 2004; 14: 86–93.
2. Inoue S, Fujikawa K, Matsuki-Fukushima M, et al. Repair processes of flat bones formed via intramembranous versus endochondral ossification. *J Oral Biosci* 2020; 62: 52–57.
3. Fu R, Liu C, Yan Y, et al. Bone defect reconstruction via endochondral ossification: a developmental engineering strategy. *J Tissue Eng* 2021; 12: 20417314211004211.
4. Douglas J. Developmental orthopaedic disease and lameness. In: Ross MW and Dyson SJ (eds) *Diagnosis and management of lameness in the Horse*. St. Louis, Mo: Elsevier Saunders, 2003, pp.534–561.
5. Park S, Bello A, Arai Y, et al. Functional duality of chondrocyte hypertrophy and biomedical application trends in osteoarthritis. *Pharmaceutics* 2021; 13: 1139.
6. Setiawati R and Rahardjo P. Bone development and growth. In: Haisheng YANG (ed.) *Osteogenesis and bone regeneration*. London: IntechOpen, 2018; p. 5772.
7. Wu YX, Jing XZ, Sun Y, et al. CD146+ skeletal stem cells from growth plate exhibit specific chondrogenic differentiation capacity in vitro. *Mol Med Rep* 2017; 16: 8019–8028.
8. Ambrosi TH, Longaker MT and Chan CKF. A revised perspective of skeletal stem cell biology. *Front Cell Dev Biol* 2019; 7: 189.
9. Thompson EM, Matsiko A, Kelly DJ, et al. An endochondral ossification-based approach to bone repair: chondrogenically primed mesenchymal stem cell-laden scaffolds support greater repair of critical-sized cranial defects than osteogenically stimulated constructs in vivo. *Tissue Eng Part A* 2016; 22: 556–567.
10. Jukes JM, Both SK, Leusink A, et al. Endochondral bone tissue engineering using embryonic stem cells. *Proc Natl Acad Sci U S A* 2008; 105: 6840–6845.
11. Black CR, Goriainov V, Gibbs D, et al. Bone tissue engineering. *Curr Mol Biol Rep* 2015; 1: 132–140.
12. Nilsson O, Marino R, De Luca F, et al. Endocrine regulation of the growth plate. *Horm Res Paediatr* 2005; 64: 157–165.
13. Khajuria DK, Razdan R and Mahapatra DR. Description of a new method of ovariectomy in female rats. *Rev Bras Reumatol* 2012; 52: 462–470.
14. Ahn T-K, Kim K-T, Joshi HP, et al. Therapeutic potential of tauroursodeoxycholic acid for the treatment of osteoporosis. *Int J Mol Sci* 2020; 21: 4274.
15. Mahmoud NS, Mohamed MR, Ali MAM, et al. Osteoblast-based therapy-a new approach for bone repair in osteoporosis: pre-clinical setting. *Tissue Eng Regen Med* 2020; 17: 363–373.
16. Kim BJ, Arai Y, Choi B, et al. Restoration of articular osteochondral defects in rat by a bi-layered hyaluronic acid hydrogel plug with TUDCA-PLGA microsphere. *J Ind Eng Chem* 2018; 61: 295–303.
17. Muttigi MS, Kim BJ, Choi B, et al. Matrilin-3-primed adipose-derived mesenchymal stromal cell spheroids prevent mesenchymal stromal-cell-derived chondrocyte hypertrophy. *Int J Mol Sci* 2020; 21: 8911.
18. Mizuhashi K, Ono W, Matsushita Y, et al. Resting zone of the growth plate houses a unique class of skeletal stem cells. *Nature* 2018; 563: 254–258.
19. Chan CK, Seo EY, Chen JY, et al. Identification and specification of the mouse skeletal stem cell. *Cell* 2015; 160: 285–298.
20. Ramos TL, Sánchez-Abarca LI, Muntión S, et al. MSC surface markers (CD44, CD73, and CD90) can identify human MSC-derived extracellular vesicles by conventional flow cytometry. *Cell Commun Signal* 2016; 14(1): 2.
21. Uder C, Brückner S, Winkler S, et al. Mammalian MSC from selected species: features and applications. *Cytometry A* 2018; 93: 32–49.
22. Deschaseaux F, Pontikoglou C and Sensébé L. Bone regeneration: the stem/progenitor cells point of view. *J Cell Mol Med* 2010; 14: 103–115.

23. Gawlitta D, Farrell E, Malda J, et al. Modulating endochondral ossification of multipotent stromal cells for bone regeneration. *Tissue Eng Part B Rev* 2010; 16: 385–395.
24. Mikael PE, Golebiowska AA, Xin X, et al. Evaluation of an engineered hybrid matrix for bone regeneration via endochondral ossification. *Ann Biomed Eng* 2020; 48: 992–1005.
25. Farrell E, Both SK, Odörfer KI, et al. In-vivo generation of bone via endochondral ossification by in-vitro chondrogenic priming of adult human and rat mesenchymal stem cells. *BMC Musculoskelet Disord* 2011; 12(1): 31.
26. Chan CKF, Gulati GS, Sinha R, et al. Identification of the human skeletal stem cell. *Cell* 2018; 175: 43–56.e21.
27. Newman P, Galenano-Niño JL, Graney P, et al. Relationship between nanotopographical alignment and stem cell fate with live imaging and shape analysis. *Sci Rep* 2016; 6: 37909.
28. Cho W, Nam SW, Lee E, et al. Comparative characterization of skeletal stem cells from various tissues. *Tissue Eng Regen Med* 2010; 7: 367–371.
29. Krebsbach PH and Robey PG. Dental and skeletal stem cells: potential cellular therapeutics for craniofacial regeneration. *J Dent Educ* 2002; 66: 766–773.
30. Kim M, Kim KH, Park SR, et al. Mesenchymal stem cells for treatment of neurological disorders: a paracrine effect. *Tissue Eng Regen Med* 2013; 10: 234–245.
31. Schlundt C, Schell H, Goodman SB, et al. Immune modulation as a therapeutic strategy in bone regeneration. *J Exp Orthop* 2015; 2: 1–10.
32. Jones BJ and McTaggart SJ. Immunosuppression by mesenchymal stromal cells: from culture to clinic. *Exp Hematol* 2008; 36: 733–741.
33. François M, Romieu-Mourez R, Li M, et al. Human MSC suppression correlates with cytokine induction of indoleamine 2,3-dioxygenase and bystander M2 macrophage differentiation. *Mol Ther* 2012; 20: 187–195.
34. Fu X, He Y, Xie C, et al. Bone marrow mesenchymal stem cell transplantation improves ovarian function and structure in rats with chemotherapy-induced ovarian damage. *Cytotherapy* 2008; 10: 353–363.
35. Chen L, Tredget EE, Wu PY, et al. Paracrine factors of mesenchymal stem cells recruit macrophages and endothelial lineage cells and enhance wound healing. *PLoS One* 2008; 3: e1886.
36. Linero I and Chaparro O. Paracrine effect of mesenchymal stem cells derived from human adipose tissue in bone regeneration. *PLoS One* 2014; 9: e107001.
37. Lo Sicco C, Reverberi D, Balbi C, et al. Mesenchymal stem cell-derived extracellular vesicles as mediators of anti-inflammatory effects: endorsement of macrophage polarization. *Stem Cells Transl Med* 2017; 6: 1018–1028.
38. Komori T. Runx2, an inducer of osteoblast and chondrocyte differentiation. *Histochem Cell Biol* 2018; 149: 313–323.
39. Nishimura R, Wakabayashi M, Hata K, et al. Osterix regulates calcification and degradation of chondrogenic matrices through matrix metalloproteinase 13 (MMP13) expression in association with transcription factor Runx2 during endochondral ossification. *J Biol Chem* 2012; 287: 33179–33190.
40. Ohba S. Hedgehog signaling in endochondral ossification. *Dev Biol J* 2016; 4: 20.
41. Gu J, Lu Y, Li F, et al. Identification and characterization of the novel Col10a1 regulatory mechanism during chondrocyte hypertrophic differentiation. *Cell death & disease* 2014; 5: e1469-e1469.
42. Wang Y, Chen H, Wang N, et al. Combined 17β-estradiol with TCDD promotes M2 polarization of macrophages in the endometriotic milieu with aid of the interaction between endometrial stromal cells and macrophages. *PLoS One* 2015; 10: e0125559.